VIP Core/Shell Nanoparticles

DOI: 10.1002/anie.201003903

Synthesis and Characterization of Multimetallic Pd/Au and Pd/Au/FePt Core/Shell Nanoparticles**

*Vismadeb Mazumder, Miaofang Chi, Karren L. More, and Shouheng Sun**

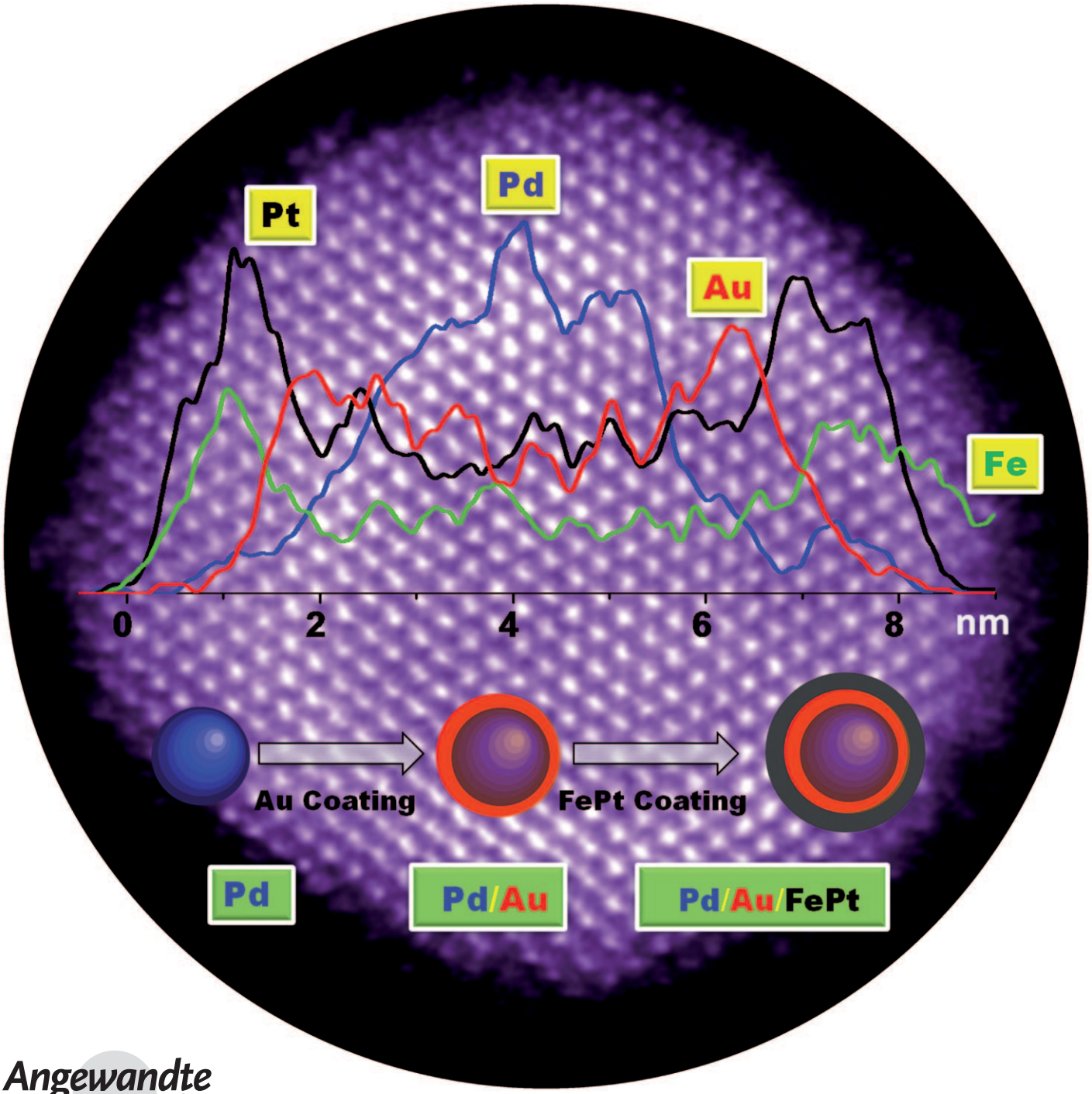

Synthesis of core/shell nanoparticles (NPs) of noble metals with tunable shell thickness is an important route to advanced nanocatalysts. Through the control of interfacial interactions between the core and the shell that are dependent on the shell thickness, core/shell NPs can be optimized for enhanced catalysis.[1] In recent synthetic advances, various methods based on solution-phase chemistry have been developed to form multimetallic core/shell NPs for potential catalytic applications. Gold or platinum core/palladium or platinum shell NPs were synthesized by a simultaneous reduction of $HAuCl_4$ and K_2PdCl_4,[2] or by the reduction of H_2PdCl_4 with ascorbic acid in the presence of Au (or Pt) NPs.[3,4] Palladium- or rhodium-rich core/shell bimetallic RhPd and PtPd NPs were formed by elemental diffusion from the respective alloy NPs.[5] Most recently, Pd/Au NPs were formed by coating Au over Pd NPs by the reduction of $HAuCl_4$ with L-ascorbic acid in the presence of Pd NPs and polyvinylpyrrolidone (PVP).[6] However, core/shell NPs reported to date were either too large (20–50 nm in diameter),[2–4] or had less control over shell thickness,[5–6] and were generally not suitable for advanced catalytic applications.

Herein we present a facile synthesis of the sub-10 nm Pd/Au NPs having a gold shell with a controlled thickness of 1–2 nm. These Pd/Au NPs can also serve as NP seeds for FePt shell coating to give quaternary Pd/Au/FePt NPs with Au and FePt forming two layers over the Pd NP core. Compared to the Au NP catalyst of similar size for oxygen reduction in 0.5 M KOH, the core/shell Pd/Au NPs are much more active, and their activities are dependent on the thickness of the gold-shell, with the thinnest (1 nm) shell exhibiting the highest activity.[7]

The core/shell Pd/Au NPs were synthesized by controlled coating of Au over Pd NPs. The synthesis was an extension to the method we developed recently for preparing core/shell Pd/FePt NPs with controlled FePt shell thickness.[8] In the synthesis, we first prepared 5 nm Pd NPs by the reduction of $[Pd(acac)_2]$ (acac = aceylacetonate) in the presence of oleylamine (OAm) and borane–*tert*-butylamine at 75 °C.[9] These Pd NPs were then used as seeds, and gold coating on palladium was achieved by reducing $HAuCl_4$ with OAm at 80 °C in the presence of Pd NPs in 1-octadecene (See Experimental Section). The average thickness of the gold coating was controlled by the amount of $HAuCl_4$ and Pd NPs added in the synthesis. Using 20 mg Pd NPs, 0.2 mmol of $HAuCl_4$ gave 5/1 nm Pd/Au NPs. Increasing the $HAuCl_4$ amount to 0.25 mmol or 0.3 mmol yielded a 1.5 or 2 nm gold coating, respectively. Under these synthetic conditions, the reduction of $HAuCl_4$ by OAm and the close (111) lattice mismatch (4%) between Pd(111) and Au(111) might facilitate the nucleation and growth of gold over the Pd NP surface. In the absence of Pd NPs, the same reaction led to the formation of polydispersed Au NPs (Supporting Information, Figure S1).

The Pd/Au NPs were initially characterized by transmission electron microscopy (TEM). Figure 1a shows the TEM image of the 5/1 nm Pd/Au NPs. The NPs have a narrow size distribution, with a standard deviation of less than 5% in the diameter. The gold coating thickness was estimated by measuring the diameter difference between the Pd/Au NPs and the seeded Pd NPs. The overall Pd/Au NP size of 7 nm indicates that the gold coating is 1 nm. The 1.5 nm and the 2 nm gold coatings over 5 nm Pd NPs were characterized similarly (Supporting Information, Figure S2). The high-resolution TEM (HRTEM) analyses further revealed the core/shell structural feature of the Pd/Au NPs. Figure 1b shows the HRTEM image of one representative 5/1 nm Pd/Au NP. Two different fringes in the core and the shell area were observed with inter-fringe distances at 0.23 nm and 0.245 nm. These fringes correspond to the (111) planes of face-centered cubic (fcc) Pd (0.223 nm) and Au (0.235 nm).

Aberration-corrected high-angle annular dark-field scanning TEM (HAADF-STEM) was then used to characterize the core/shell NPs. Its image measures the contrast variations that are proportional to the square of the atomic number of an element, and can provide key information regarding the elemental distribution within nanostructures at sub-Ångstrom resolution.[10] Figure 1c,d show the representative HAADF-STEM image of the 5/1 nm Pd/Au NPs; the gold shell is brighter owing to its heavier atomic weight, whereas the palladium core is darker. The core sizes and shell thicknesses were measured to be (4.9 ± 0.8) nm/(0.9 ± 0.1) nm based on an average measurement from 40 NPs. The compositional architecture of these core/shell NPs was further supported by high-resolution energy dispersive spectroscopy (EDS). The high-resolution EDS result for a typical 5/1 nm Pd/Au NP is given in Figure 1e,f. The elemental variation across points 1–4 of the core/shell NP is consistent with the observations made by TEM and HAADF-STEM images. Palladium is observed only at points 2 and 3 in the core (darker image) area of the 5/1 nm Pd/Au NP.

The as-synthesized Pd/Au NPs can also serve as seeds for FePt coating to give quaternary Pd/Au/FePt NPs, with Au and FePt forming two distinct metallic layers over the Pd NP core. The 2 nm FePt coating over the 5/1 nm Pd/Au NPs was achieved by controlled reduction of $[Pt(acac)_2]$ (0.175 mmol) and thermal decomposition of iron pentacarbonyl ($[Fe(CO)_5]$, 0.07 mL, 0.5 mmol) in the presence of OAm (6 mmol), oleic acid (3 mmol), and Pd/Au NPs (20 mg) in 1-octadecene solvent (8 mL; see Experimental Section). The FePt composition within the core/shell NPs was quantified by inductively coupled plasma atomic emission spectroscopy (ICP-AES). The FePt shell in these 5/1/2 nm Pd/Au/FePt NPs has a composition of $Fe_{38}Pt_{62}$. In the synthesis, the key points to achieving successful FePt coating over the Pd/Au NPs were

[*] V. Mazumder, Prof. S. Sun
Department of Chemistry, Brown University
Providence, RI 02912 (USA)
E-mail: ssun@brown.edu
Dr. M. Chi, Dr. K. L. More
Oak Ridge National Laboratory
Oak Ridge, TN 37831 (USA)

[**] Partially supported by the U.S. Department of Energy, Office of Energy Efficiency and Renewable Energy, Fuel Cell Technologies Program. Research at the ORNL SHaRE User Facility was supported by the Division of Scientific User Facilities, Office of Basic Energy Sciences, Office of Science, U.S. Department of Energy.

Supporting information for this article is available on the WWW under http://dx.doi.org/10.1002/anie.201003903.

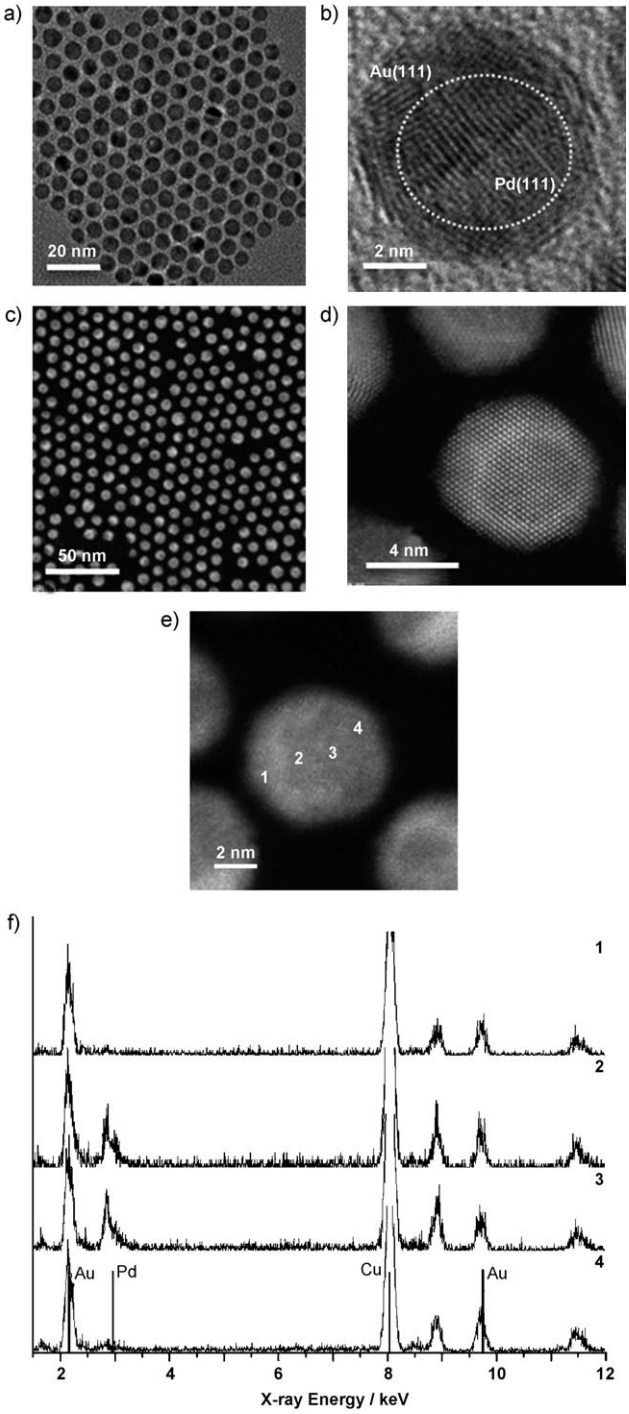

Figure 1. a–d) Representative TEM (a), HR-TEM (b), STEM (c), and high-resolution HAADF-STEM (d) images of the 5/1 nm Pd/Au NPs. e) Representative HAADF-STEM image and f) HR-STEM-EDS analysis of a single 5/1 nm Pd/Au NP at points indicated in (e).

the ratio of Pd/Au NPs and Pt salt and also the use of $[Fe(CO)_5]$. Too much variation in their amounts caused separate nucleation and growth of platinum- and/or iron-based NPs. Without $[Fe(CO)_5]$, platinum could not nucleate on the Pd/Au seeds. Rather, Pt NPs were formed separately and precipitated out from the reaction solution. An excess of $[Fe(CO)_5]$ or higher reaction temperatures led to the formation of the mixture of Pt NPs and dumbbell-like Pd/Au-Fe_3O_4 NPs (Supporting Information, Figure S3).

The Pd/Au/FePt NPs were characterized by TEM, HAADF-STEM, and high-resolution EDS line scans. The NPs have an average size of 11 nm (Figure 2a). The HAADF-STEM image (Figure 2b) reveals the darker palladium core and brighter Au/FePt shell. The close atomic weight of gold and platinum makes the Au sub-shell and FePt shell indistinguishable. To verify the Au and FePt shell thickness, high-resolution EDS line-scans across the NP were obtained. The full-width at half-maximum (FWHM) of the EDS intensity profiles of elemental Pd, Au, Fe, and Pt were plotted as a function of the cross-section distance (Figure 2c). Based on an average of 10 NPs, the FePt shell thickness was

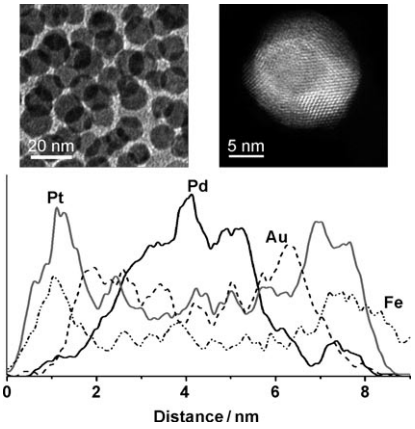

Figure 2. a,b) Representative TEM (a) and HR-HAADF-STEM (b) image of a single 5/1/2 nm Pd/Au/FePt NP. c) High-resolution line-scan EDS analysis across the NP. The analysis was obtained by scanning 150 points with a beam size of about 2 Å.

measured to be (2 ± 0.4) nm and the Au sub-shell was (1.1 ± 0.2) nm. From the line scans, we see no obvious overlap between Au and FePt layers, indicating that there is no measurable interatomic diffusion between Au and FePt layers. These results further confirm that our synthesis yields a layer-by-layer growth in the formation of the Pd/Au/FePt structure.

The controlled coating of Au over Pd NPs and FePt over Pd/Au NPs were further characterized by X-ray diffraction (XRD) patterns and UV/Vis spectroscopy of the related core/shell structures. Figure 3a shows the UV/Vis spectra of the Pd, Au, and Pd/Au NPs in hexane dispersions. In the studied wavelength range, the 5 nm Pd NPs have no surface plasmon resonance (SPR) absorption, and the 6 nm Au NPs, synthesized from $HAuCl_4 \cdot 3H_2O$ reduction by borane–*tert*-butylamine in the presence of oleylamine,[7] have the typical SPR absorption at 520 nm. The SPR absorptions of the Au shells in the Pd/Au NPs are dependent on the Au shell thickness, with the 2 nm shell showing a stronger absorption than the 1 nm shell, but their absorptions are much weaker than the free Au NPs. The Au SPR disappears in Pd/Au/FePt NPs owing to the FePt coating over Pd/Au. Figure 3b shows the XRD patterns of the 5 nm Pd, 5/1 nm Pd/Au NPs, and 5/1/2 nm Pd/Au/FePt NPs. The (111) peak is at 39° for the Pd NPs. The

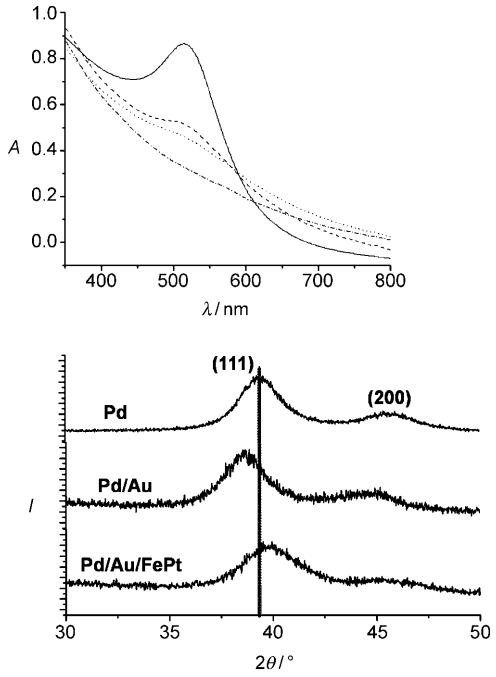

Figure 3. a) UV/Vis spectra of the 5 nm Pd (–•–•–), 6 nm Au (——), 5/1 nm Pd/Au (•••••), and 5/2 nm Pd/Au (-----) NPs in hexane dispersions. b) XRD analysis of the 5 nm Pd, 5/1 nm Pd/Au, and 5/1/2 nm Pd/Au/FePt NPs.

peak shifts to 38° for the Pd/Au NPs and 40° for the Pd/Au/FePt NPs, which is similar to those of Au(111) and FePt(111), respectively. These values indicate that the core/shell structures are indeed formed.

The controlled gold coating over palladium also allows Pd/Au NPs to be formed with the desired structural tunability for studying shell-thickness-dependent catalysis. We chose to investigate their catalytic oxygen reduction reaction (ORR) in 0.5 M KOH, which is a common condition used to evaluate catalyst activity in alkaline fuel cells. To perform the catalysis tests, we deposited the Pd/Au NPs on a Ketjen carbon support ($800\ m^2 g^{-1}$) by sonification of 10 mg of each of the two constituents in 5 mL hexane and 5 mL acetone for one hour. After the evaporation of acetone–hexane solvent, the dried Pd/Au/C samples were re-dispersed in deionized water to give a 2 mg NPs/mL solution. We prepared three Pd/Au/C NP catalysts, each having the same 5 nm palladium core and differing by the thickness of the gold coatings (1, 1.5 nm, and 2 nm).

20 μL of each of the three Pd/Au/C water dispersions was deposited on the glassy carbon surface of a rotating disk electrode (RDE) for ORR studies in O_2-saturated 0.5 M KOH at 298 K. The current generated from the ORR at 1600 rpm was normalized by dividing the measured raw electrode currents with the mass of NPs (40 μg; see the Experimental Section). Figure 4 summarizes the observed ORR current for three Pd/Au NP catalysts. The 5/1 nm Pd/Au NPs have slightly better activity than the 5/1.5 nm Pd/Au NPs, but have a 150 mV gain in onset potential than the 5/2 nm Pd/Au NPs and are 75 mV better than that from the 6 nm Au NP catalysts.[7] Clearly, the Pd/Au NPs with gold shells thinner

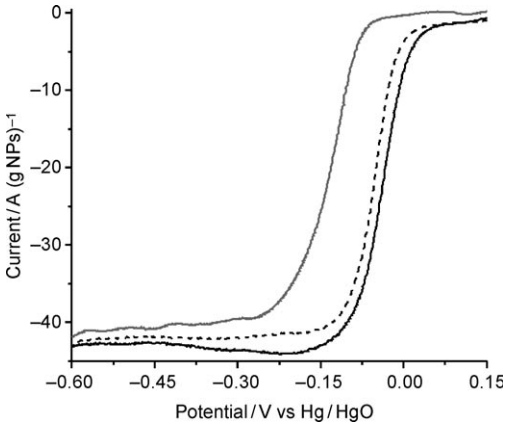

Figure 4. Polarization curves showing the oxygen reduction reaction current for three different Pd/Au NPs having 1 nm (——), 1.5 nm (-----), and 2 nm (——) coatings. The current was standardized against the total mass of NPs (40 μg) used, and the electrode rotation rate was kept at 1600 rpm.

than 1.5 nm are much more active than those with a 2 nm gold coating.

In conclusion, we have presented a facile synthesis of multimetallic core/shell NPs of Pd/Au and Pd/Au/FePt. With a 5 nm Pd NP core, the gold shell has a controlled 1–2 nm thickness and the FePt shell is 2 nm thick. For Pd/Au NPs, preliminary studies on their catalytic ORR in 0.5 M KOH indicate that Pd/Au NPs with a gold shell thinner than 1.5 nm are much more active than those with 2 nm shell and pure Au NPs. The work demonstrates that catalytic property of the Pd/Au NPs can indeed be tuned by the shell thickness. Our synthesis is versatile and should allow an even greater variety of metals to be incorporated into either the core or the shell structure. It opens up new vistas to exploit core/shell interactions for future development of multicomponent NPs with unprecedented activities for catalytic applications.

Experimental Section

The syntheses were carried out using standard airless procedures and commercially available reagents. Oleylamine (>70%), oleic acid, platinum(II) acetylacetonate, palladium(II) acetylacetonate, iron pentacarbonyl, palladium(II) bromide, acetic acid, borane–*tert*-butylamine complex, and Nafion solution were all purchased from Sigma Aldrich.

Synthesis of core/shell 5/1 nm Pd/Au NPs: $HAuCl_4 \cdot 3H_2O$ (0.2 mmol) was dissolved in 1-octadecene (8 mL) and oleylamine (2 mL). The resultant orange solution was slowly heated to 80 °C, and the Pd NP seeds (20 mg) dispersed in hexanes (2 mL) were injected into the solution. The reaction mixture was kept at the same temperature for 2 h and then cooled down to room temperature. Isopropanol (40 mL) was added and the suspension was centrifuged at 8000 rpm to separate the solid product. The product was dispersed in hexane (30 mL) and precipitated out by adding ethanol (40 mL). The final product, 5/1 nm Pd/Au NPs, was dispersed in hexanes (5 mL) for further use.

By tuning the amount of Au precursor used, Pd/Au NPs with different Au shell thickness were synthesized: the 1.5 nm Au shell was obtained from 0.25 mmol of Au precursor, and the 2 nm shell was formed from 0.3 mmol of Au precursor.

Synthesis of 5/1/2 nm Pd/Au/FePt NPs: 70 mg of $[Pt(acac)_2]$ was mixed with 1-octadecene (8 mL), oleylamine (2 mL), and oleic acid (1 mL). This solution was heated to 120 °C at a rate of 6–7 °C min^{-1}, and 5/1 nm Pd/Au NPs (20 mg) dispersed in hexane (2 mL) was injected into the reaction mixture. The reaction mixture was heated to 125 °C and $[Fe(CO)_5]$ (0.07 mL) was added under a nitrogen blanket. The mixture was heated at 5 °C min^{-1} to 200 °C and was kept at this temperature for 20 min. The mixture was cooled down to room temperature. Isopropanol (40 mL) was added to precipitate out the product. The NPs were separated as described in the synthesis of Pd/Au NPs and dispersed in hexanes.

Samples for TEM analysis were prepared by depositing a single drop of diluted NP dispersion in hexane on amorphous carbon-coated copper grids. Images were obtained by a Philips EM 420 (120 kV). HRTEM image was obtained on a JEOL 2010 TEM (200 kV). XRD patterns were obtained on a Bruker AXS D8-Advanced diffractometer with $Cu_{K\alpha}$ radiation ($\lambda = 1.5418$ Å). ICP measurements were carried on a JY2000 Ultrace ICP atomic emission spectrometer equipped with a JY AS 421 autosampler and 2400 g mm^{-1} holographic grating.

High-resolution STEM and EDS analyses were carried out on an aberration-corrected JEOL 2200FS microscope. HAADF-STEM images were acquired with a convergence angle of 27 mrad and an inner collection angle of 100 mrad. Bright-field STEM (BF-STEM) images were recorded simultaneously with HAADF-STEM images to obtain complete information of the microstructures. EDS analysis was carried out with an electron beam size of about 2 Å. Before conducting any measurements, the NP samples were tested against possible electron-beam-induced damage; no damage was observed under the STEM operational conditions.

Electrochemical measurements were performed on a Pine Electrochemical Analyzer, Model AFCBP1, by cyclic voltammetry (CV). Hg/HgO and Pt wire were used as reference and counter-electrodes, respectively. The oxygen reduction reaction (ORR) catalyzed by the NP catalysts was evaluated in the O_2-saturated 0.5 M KOH at 298 K. The rotating disk electrode (RDE) rotation speed was controlled over the range 1225–2500 rpm and the scan rate was at 10 mV s^{-1} in the 0.2 V to −0.6 V region scanned. The current (A g^{-1} NPs) originating from ORR was standardized by dividing the measured electrode currents with the mass of the total metal content of the 50 % NP/C catalyst (40 μg).

Received: June 28, 2010
Published online: September 17, 2010

Keywords: core/shell particles · gold · heterogeneous catalysis · nanoparticles · palladium

[1] a) X. Peng, M. C. Schlamp, A. V. Kadavanich, A. P. Alivisatos, *J. Am. Chem. Soc.* **1997**, *119*, 7019–7029; b) M. C. Schlamp, X. G. Peng, A. P. Alivisatos, *J. Appl. Phys.* **1997**, *82*, 5837–5842; c) C. J. Zhong, M. M. Maye, *Adv. Mater.* **2001**, *13*, 1507–1511; d) J. X. Wang, H. Inada, L. Wu, Y. Zhu, Y. Choi, P. Liu, W.-P. Zhou, R. R. Adzic, *J. Am. Chem. Soc.* **2009**, *131*, 17298–17302.
[2] a) J. Luo, L. Wang, D. Mott, P. N. Njoki, Y. Lin, T. He, Z. Xu, B. N. Wanjana, I.-I. S. Lim, C.-J. Zhong, *Adv. Mater.* **2008**, *20*, 4342–4347; b) Y. W. Lee, M. Kim, Z. H. Kim, S. W. Han, *J. Am. Chem. Soc.* **2009**, *131*, 17036–17038.
[3] S. E. Habas, H. Lee, V. Radmilovic, G. A. Somorjai, P. Yang, *Nat. Mater.* **2007**, *6*, 692–697.
[4] F. Fan, D. Liu, Y. Wu, S. Duan, Z. Xie, Z. Jiang, Z. Tian, *J. Am. Chem. Soc.* **2008**, *130*, 6949–6951.
[5] F. Tao, M. E. Grass, Y. Zhang, D. R. Butcher, J. R. Renzas, Z. Liu, J. Y. Chung, B. S. Mun, M. Salmeron, G. A. Somorjai, *Science* **2008**, *322*, 932–935 .
[6] B. Lim, H. Kobayashi, T. Yu, J. Wang, M. J. Kim, Z. Li, M. Rycenga, Y. Xia, *J. Am. Chem. Soc.* **2010**, *132*, 2506–2507.
[7] Y. Lee, A. Loew, S. Sun, *Chem. Mater.* **2010**, *22*, 755–761.
[8] V. Mazumder, M. Chi, K. L. More, S. Sun, *J. Am. Chem. Soc.* **2010**, *132*, 7848–7849.
[9] V. Mazumder, S. Sun, *J. Am. Chem. Soc.* **2009**, *131*, 4588–4589.
[10] a) E. J. Kirkland, R. F. Loane, J. Silcox, *Ultramicroscopy* **1987**, *23*, 77–91; b) P. D. Nellist, S. J. Pennycock, *Ultramicroscopy* **1999**, *78*, 111–123.

